

Cite this: DOI: 10.1039/c2cc37109j

www.rsc.org/chemcomm

A Ni@ZrO₂ nanocomposite for ethanol steam reforming: enhanced stability *via* strong metal–oxide interaction†‡

Shuirong Li, Chengxi Zhang, Zhiqi Huang, Gaowei Wu and Jinlong Gong*

Received 30th September 2012, Accepted 22nd October 2012

DOI: 10.1039/c2cc37109j

This communication describes the synthesis of a nanocomposite Ni@ZrO₂ catalyst with enhanced metal–support interaction by introducing metal nanoparticles into the framework of the oxide support. The catalyst shows high catalytic activity and stability for hydrogen production *via* steam reforming of ethanol.

Hydrogen production from renewable resources represents a hot research topic of the last few decades.¹ Supported nickel catalysts are industrially used for hydrogenation and steam reforming, and have been investigated intensively for many years. Due to their high activity in C–C bond rupture and low cost, nickel catalysts have been also proposed recently as promising candidates in ethanol steam reforming (ESR) for hydrogen production. However, deactivation with time on stream primarily caused by sintering and coke deposition remains an unsolved drawback of this type of catalysts in reforming processes including ESR.²

Stabilization of nickel nanoparticles by solid-phase crystallization and enhancing the removal of surface carbon deposits by the introduction of oxides with high oxygen mobility are two typical approaches for the improvement of catalytic stability of supported catalysts in ESR.³ Nickel catalysts prepared from crystalline oxide precursors, such as hydroxalcalite compounds,⁴ perovskite,⁵ and spinel,⁶ show enhanced metal dispersion and metal–support interaction; this, in turn, improves catalytic activity and stability in ESR. Oxides with high oxygen mobility—typically rare-earth metal oxides—were reported to be beneficial for the activation of steam as well as the removal of surface carbon deposits in reforming.⁷ Recent attention has been paid to the removal of surface carbon deposit on catalysts derived from crystalline oxide precursors.⁸ However, limited work was reported regarding the improvement of sintering resistance of catalysts supported on oxides with high surface oxygen mobility.⁹

Zirconia is widely used as a catalytic support for its amphoteric character as well as thermal and chemical stability.¹⁰ It is also favored in reforming processes for its moderate

acidity¹¹ and surface oxygen mobility.¹² Xu *et al.* proposed a “size effect” of the zirconia support and found that the reduction in particle size of zirconia would result in increased surface area, metal dispersion, as well as strengthened metal–support interaction; these features would thus enhance catalytic performance of nickel particles supported on ZrO₂ in dry reforming of methane.¹³ However, for catalysts prepared by conventional impregnation, metal particles were set on a bulk matrix composite of substrate oxide particles with fixed-frame structure (Fig. 1a). Under heat treatment, metal particles would suffer from sintering and grow up readily. Ideally, if frame structure of the catalyst is composed of comparable nanosized metal particles and support oxide particles (Fig. 1b), the metal particles would help in the construction of the pore structure instead of blocking it resulting in an increased surface area. Since the amount of substrate oxide particles is dominant in the catalyst, each metal nanoparticle would be confined by several surrounding oxide particles. Accordingly, the metal–support interaction in the catalyst could be strengthened with increased interfacial area, expectedly leading to improved catalytic performance of the catalyst in the reforming process.¹⁴

To prepare such a catalyst, nanosized metal particles or their precursors are needed during the construction of a substrate matrix. Considering that metallic Ni is prone to oxidation in air and to avoid the use of hydrazine as a reduction reagent,¹⁵ NiO nanoparticles were used in the preparation of Ni@ZrO₂ nanocomposites. NiO nanoparticles with a particle size of about 3.3 ± 0.7 nm (Table 1, Fig. S1, ESI†) were prepared by a surfactant-assisted route¹⁶ while the Ni@ZrO₂ nanocomposite (15 wt% Ni loading) was synthesized by a modified hydrothermal method in the presence of as-prepared NiO

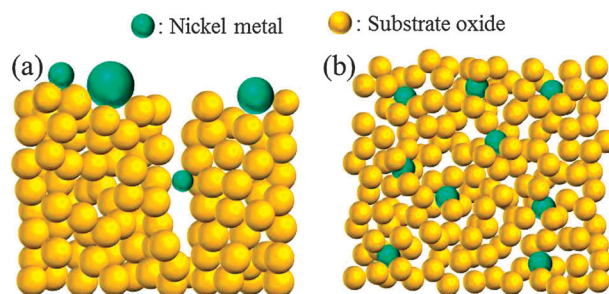


Fig. 1 Schematic illustration of (a) conventional supported metal catalyst, and (b) nanoconfined metal–oxide composite.

Key Laboratory for Green Chemical Technology of Ministry of Education, School of Chemical Engineering and Technology, Tianjin University, Tianjin 300072, China. E-mail: jlgong@tju.edu.cn; Fax: +86 22 87401818

† This article is part of the *ChemComm* ‘Emerging Investigators 2013’ themed issue.

‡ Electronic supplementary information (ESI) available: Experimental details and physico-chemical properties of supported nickel catalysts. See DOI: 10.1039/c2cc37109j

Table 1 Physico-chemical properties of nickel catalysts

Sample	$S_{\text{BET}}/\text{m}^2 \text{g}^{-1}$	$V_{\text{Pore}}/\text{cm}^3 \text{g}^{-1}$	$D_{\text{Pore}}/\text{nm}$	Particle size ^a		Dispersion ^b / $\text{m}^2 \text{g}_{\text{Ni}}^{-1}$
				Ni	ZrO ₂	
NiO	210	0.47	7.6	N.A.	N.A.	N.A.
ZrO ₂	47	0.11	6.7	N.A.	13.0	N.A.
Ni/ZrO ₂	40	0.15	11.3	23.7	15.7	1.7
Ni@ZrO ₂	91	0.33	11.2	10.5	9.2	7.0

^a Calculated from the peak broadenings of Ni(111), m-ZrO₂(111), and t-ZrO₂(011) using the Scherrer equation, respectively. ^b Calculated from the H₂ pulse chemisorption.

nanoparticles during the gelation of the ZrO₂ precursor. For comparison, the supported Ni/ZrO₂ catalyst (15 wt%) was also fabricated by a conventional impregnation method (see ESI† for details). Both of the catalysts were activated in a reducing stream of H₂/N₂ (10 ml/40 ml) at 773 K for 1 h prior to catalytic activity tests.

Physico-chemical properties of the as synthesized nickel catalysts are listed in Table 1 and Fig. 2. Physisorption of N₂ showed that the specific surface area of the Ni@ZrO₂ catalyst is more than twice larger than that of the conventionally supported one. The formation of different crystalline phases of zirconia as indicated in their XRD patterns (Fig. 2a) could account for this disparity.¹⁰ Peaks at 28.2° and 31.5° indicate the domination of monoclinic zirconia (m-ZrO₂) in the pure ZrO₂ and the supported Ni/ZrO₂ catalyst, while the peak at 30.3° indicates the presence of a metastable phase of zirconia in Ni@ZrO₂. Although XRD could not effectively distinguish tetragonal zirconia (t-ZrO₂) from cubic zirconia (c-ZrO₂), t-ZrO₂ rather than c-ZrO₂ was believed to be stabilized by the possible presence of Ni²⁺ during the precipitation of the ZrO₂ precursor with the coexistence of the ammonia precipitator and

NiO nanoparticles.¹⁷ The domination of t-ZrO₂ could partially contribute to the higher surface area of the Ni@ZrO₂ catalyst.¹⁰ However, the surface area of ZrO₂ prepared by the precipitation method is generally lower than 50 m² g⁻¹.¹⁸ It is noticed that both catalysts prepared using a similar method showed a similar pore diameter while the Ni@ZrO₂ catalyst possesses a much larger volume of the mesopore structure compared to the Ni/ZrO₂ catalyst. This could also be the evidence of the formation of designed structure of the Ni@ZrO₂ nanocomposite, in which NiO nanoparticles substitute part of ZrO₂ particles in the matrix instead of blocking its pore structures.

The formation of proposed structure is further evidenced by electron microscopy analysis. For the supported Ni/ZrO₂ catalyst (Fig. 2c), particles with size ranging from 16 to 50 nm were distributed both at the edge and the inside of another aggregation of small particles (about 15 nm). EDX images of selected areas of the sample (Fig. S1, ESI†) attribute the large particles to nickel, which was further confirmed by the STEM analysis (see the inset in Fig. 2c). As for the nanocomposite Ni@ZrO₂ catalyst, only a mixture of comparably nanosized particles was observed; STEM images (the inset in Fig. 2d) of selected area show that small nickel particles were uniformly distributed within the ZrO₂ matrix.

The surface interaction between NiO and ZrO₂ of the catalysts was evaluated by H₂-TPR experiments (Fig. 2b). A reduction peak at 579 K and a shoulder peak at 693 K were observed for the supported Ni/ZrO₂ catalyst, whereas only an intense reduction peak at about 723 K was detected for the nanocomposite Ni@ZrO₂ catalyst. Concerning that the formation of strong chemical bonds between the Ni metal and the ZrO₂ has been revealed based on a DFT calculation by Beltran,¹⁹ the reduction peak at 579 K was attributed to the reduction of bulk NiO²⁰ while the reduction peaks at 693–723 K were related to NiO_x species that have strong interaction with ZrO₂. The strengthened interaction between the nickel metal and the zirconia could be probably due to an increased interfacial area.¹⁹

We should note that a high metal dispersion was also obtained over the nanocomposite Ni@ZrO₂ catalyst. This could be directly evidenced by the TEM/STEM images of the reduced nickel catalysts, in which more uniform and smaller particles of the nickel metal were observed over the Ni@ZrO₂ catalyst compared to Ni/ZrO₂ (Fig. 2c and d). Average Ni particle sizes of 10.5 nm and 23.7 nm for Ni@ZrO₂ and Ni/ZrO₂ calculated based on the Ni(111) diffraction peaks (Table 1) also confirm this observation. For quantitative analysis, H₂-TPD experiments (see ESI† for details) were also performed over the nickel catalysts. The results showed a metal surface area of 7.0 m² g_{Ni}⁻¹ for the nanocomposite Ni@ZrO₂ catalyst, which is four times more than that of the supported one (Table 1).

According to the ESR mechanism, the metal activates the organic molecules and promotes their reaction with OH groups provided by water dissociation on the support.²¹ A catalyst with higher metal dispersion and metal-support interfacial area is thus expected to offer a better performance in ESR. A relatively low temperature (*i.e.* 723 K) was selected for catalytic activity tests of the nickel catalysts. Varying the gas hour space velocity (GHSV) would allow us through the changes in conversion

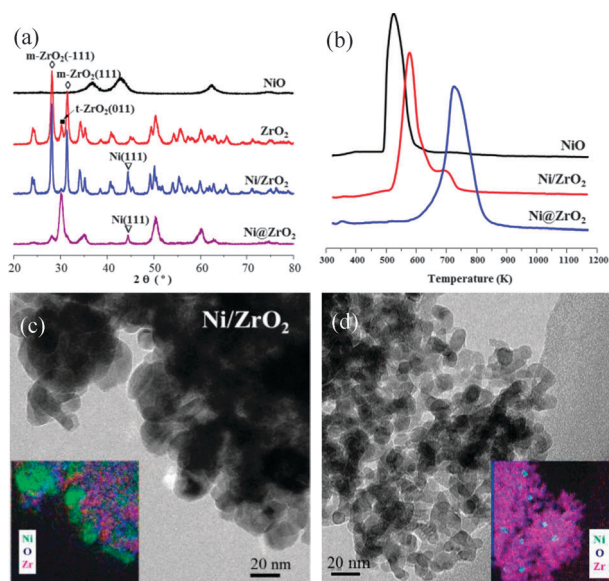


Fig. 2 (a) XRD patterns of as prepared NiO, ZrO₂, reduced Ni/ZrO₂, and Ni@ZrO₂. (b) H₂-TPR profiles of NiO, Ni/ZrO₂ and Ni@ZrO₂ catalysts. TEM images of (c) reduced Ni/ZrO₂ and (d) reduced Ni@ZrO₂. The insets in (c) and (d) correspond high-angle annular dark field (HAADF) STEM images of the reduced nickel catalysts.

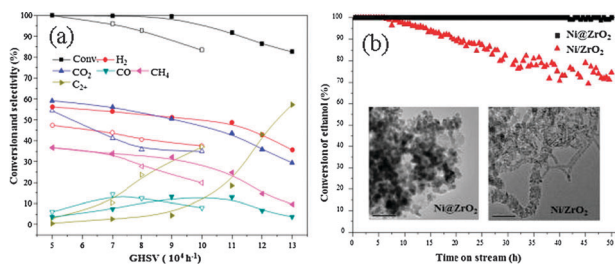


Fig. 3 (a) Catalytic activity at 723 K. Solid symbols: Ni@ZrO₂ catalyst; hollow symbols: Ni/ZrO₂ catalyst. (b) Catalytic stability at 873 K. The insets are TEM images of the used catalysts.

of ethanol and selectivity of the products to compare the catalytic activities of the synthesized nickel catalysts. As shown in Fig. 3a, the decrease in ethanol conversion as well as the emergence of C₂+ products (mainly acetaldehyde and a trace amount of acetone) with an increase in GHSV could be clues of insufficient catalytic activity of the conventional supported Ni/ZrO₂ catalyst for C–H and C–C bonds cleavage under given conditions.² Comparatively, a similar phenomenon was only detected at higher GHSV for the nanocomposite Ni@ZrO₂ catalyst, indicating a higher activity towards ethanol activation and conversion into C₁ species on its surface. In addition, the Ni@ZrO₂ catalyst shows a higher selectivity towards H₂ and CO₂ production, which could be partially attributed to a higher WGS activity promoted by the stabilized tetragonal zirconia²² as well as the prolonged metal–support interface.¹⁴

The catalytic stability of the nickel catalysts was also investigated as a function of time on stream over a period of 50 h, at 873 K and a GHSV of 50 000 h⁻¹, as depicted in Fig. 3b. The nanocomposite Ni@ZrO₂ catalyst showed a nearly complete conversion of ethanol during the entire testing period, whereas a continual decrease in ethanol conversion after 6 h of reaction was observed over the supported Ni/ZrO₂ catalyst. Two major factors could contribute to the excellent stability of the Ni@ZrO₂ catalyst: (i) the geometric confinement of the surrounding comparable nanosized zirconia particles and strong interaction between the nickel metal and zirconia that prevent the nickel metal from sintering,²³ and (ii) the richness of surface active oxygen²⁴ and prolonged metal–support interfacial perimeter that help in the removal of carbon deposits.²⁵ Ni particle size of the used Ni@ZrO₂ is nearly intact (*i.e.* 10.8 nm) based on the calculation using the Scherrer formula from its XRD pattern (Fig. S2a, ESI†), while an apparent increase in nickel size (*i.e.* 25.4 nm) was found for the used Ni/ZrO₂ catalyst. TEM images (the inset of Fig. 3b and Fig. S2c and S2d in ESI†) exhibit that only some amorphous carbon was formed over the used Ni@ZrO₂, while a large amount of carbon whiskers was observed for the used Ni/ZrO₂ catalyst. TG measurements performed upon the stability tests (Fig. S2b, ESI†) indicate weight losses of 16.9% and 33.7% for the used Ni@ZrO₂ and Ni/ZrO₂ catalysts, respectively.

In summary, we have demonstrated the successful design of a novel nickel–zirconia nanocomposite for hydrogen production *via* steam reforming of ethanol. The introduction of nickel particles into the framework of an oxide support with high oxygen mobility could effectively maintain the pore structure of the oxide support and increase the accessibility of the metal

particles. Particularly, the size match of the metal and oxide could increase the metal–oxide interface length and strengthen their interaction. Additionally, the confinement effect could effectively prevent metal particles from sintering. The methodology reported here may be useful for designing other types of metal catalysts that are prone to deactivation due to sintering and/or coke deposition under realistic conditions for reactions such as reforming, methanation, and dehydrogenation.

We thank the National Natural Science Foundation of China (21006068, 21206115, 21222604), the Program for New Century Excellent Talents in University (NCET-10-0611), the Scientific Research Foundation for the Returned Overseas Chinese Scholars (MoE), Seed Foundation of Tianjin University (60303002), the Program of Introducing Talents of Discipline to Universities (B06006), and China Postdoctoral Science Foundation for their generous support.

Notes and references

- 1 D. Merki, S. Fierro, H. Vrubel and X. Hu, *Chem. Sci.*, 2011, **2**, 1262.
- 2 L. V. Mattos, G. Jacobs, B. H. Davis and F. B. Noronha, *Chem. Rev.*, 2012, **112**, 4094.
- 3 F. Aupretre, C. Descorme, D. Duprez, D. Casanave and D. Uzio, *J. Catal.*, 2005, **233**, 464.
- 4 G. Wu, C. Zhang, S. Li, Z. Huang, S. Yan, S. Wang, X. Ma and J. Gong, *Energy Environ. Sci.*, 2012, **5**, 8942.
- 5 S. M. de Lima, A. M. da Silva, L. O. O. da Costa, J. M. Assaf, L. V. Mattos, R. Sarkari, A. Venugopal and F. B. Noronha, *Appl. Catal., B*, 2012, **121–122**, 1.
- 6 H. Muroyama, R. Nakase, T. Matsui and K. Eguchi, *Int. J. Hydrogen Energy*, 2010, **35**, 1575.
- 7 A. N. Fatsikostas and X. E. Verykios, *J. Catal.*, 2004, **225**, 439.
- 8 A. E. Galetti, M. F. Gomez, L. A. Arrua and M. C. Abello, *Appl. Catal., A*, 2011, **408**, 78.
- 9 G. Zhou, L. Barrio, S. Agnoli, S. D. Senanayake, J. Evans, A. Kubacka, M. Estrella, J. C. Hanson, A. Martinez-Arias, M. Fernandez-Garcia and J. A. Rodriguez, *Angew. Chem., Int. Ed.*, 2010, **49**, 9680.
- 10 T. Yamaguchi, *Catal. Today*, 1994, **20**, 199.
- 11 Z. Zhong, H. Ang, C. Choong, L. Chen, L. Huang and J. Lin, *Phys. Chem. Chem. Phys.*, 2009, **11**, 872.
- 12 V. Nichele, M. Signoretto, F. Menegazzo, A. Gallo, V. Dal Santo, G. Cruciani and G. Cerrato, *Appl. Catal., B*, 2012, **111**, 225.
- 13 B.-Q. Xu, J.-M. Wei, Y.-T. Yu, Y. Li, J.-L. Li and Q.-M. Zhu, *J. Phys. Chem. C*, 2003, **107**, 5203.
- 14 S. Li, M. Li, C. Zhang, S. Wang, X. Ma and J. Gong, *Int. J. Hydrogen Energy*, 2012, **37**, 2940.
- 15 D. H. Chen and S. H. Wu, *Chem. Mater.*, 2000, **12**, 1354.
- 16 J.-H. Li, C.-C. Wang, C.-J. Huang, Y.-F. Sun, W.-Z. Weng and H.-L. Wan, *Appl. Catal., A*, 2010, **382**, 99.
- 17 G. Štefanić, M. Didović and S. Musić, *J. Mol. Struct.*, 2007, **834–836**, 435.
- 18 K. T. Jung, Y. G. Shul and A. T. Bell, *Korean J. Chem. Eng.*, 2001, **18**, 992.
- 19 J. I. Beltran, S. Gallego, J. Cerdá, J. S. Moya and M. C. Muñoz, *Phys. Rev. B*, 2003, **68**, 075401.
- 20 S. Tomiyama, R. Takahashi, S. Sato, T. Sodesawa and S. Yoshida, *Appl. Catal., A*, 2003, **241**, 349.
- 21 H. Idriss, *Platinum Met. Rev.*, 2004, **48**, 105.
- 22 G. Aguila, S. Guerrero and P. Araya, *Catal. Commun.*, 2008, **9**, 2550.
- 23 P.-Z. Li, K. Aranishi and Q. Xu, *Chem. Commun.*, 2012, **48**, 3173.
- 24 X. Zhang, H. Shi and B.-Q. Xu, *J. Catal.*, 2011, **279**, 75.
- 25 (a) C. Zhang, S. Li, M. Li, S. Wang, X. Ma and J. Gong, *AIChE J.*, 2012, **58**, 516; (b) L. Zhang, Y. Ren, B. Yue and H. He, *Chem. Commun.*, 2012, **48**, 2370.